JACS
JOURNAL OF THE AMERICAN CHEMICAL SOCIETY
Communication
pubs.acs.org/JACS

Highly Active Mixed-Metal Nanosheet Water Oxidation Catalysts Made by Pulsed-Laser Ablation in Liquids

Bryan M. Hunter, James D. Blakemore, Mark Deimund, Harry B. Gray, Jay R. Winkler, and Astrid M. Müller*

Beckman Institute and Division of Chemistry and Chemical Engineering, California Institute of Technology, M/C 139-74, Pasadena, California 91125, United States

Supporting Information

ABSTRACT: Surfactant-free mixed-metal hydroxide water oxidation nanocatalysts were synthesized by pulsed-laser ablation in liquids. In a series of [Ni-Fe]-layered double hydroxides with intercalated nitrate and water, $[Ni_{1-x}Fe_x(OH)_2](NO_3)_y(OH)_{x-y}{\cdot}nH_2O$, higher activity was observed as the amount of Fe decreased to 22%. Addition of Ti^{4+} and La^{3+} ions further enhanced electrocatalysis, with a lowest overpotential of 260 mV at 10 mA cm^{-2}. Electrocatalytic water oxidation activity increased with the relative proportion of a 405.1 eV N 1s (XPS binding energy) species in the nanosheets.

Conversion of solar energy into storable fuels in a sustainable way will be essential to meet future global energy demands. Worldwide scalability requires materials to be made from earth-abundant elements. Splitting water into oxygen and hydrogen with only sunlight as energy input is seen as a particularly attractive route.[1] But such systems for the production of solar fuels will require robust, highly active catalysts.[2−4]

Most widely used water oxidation catalysts are based on rare metals such as Ru and Ir.[5,6] First-row transition metal oxides and hydroxides continue to attract attention because of their low cost and stability in base.[7−14] The overpotentials of earth-abundant catalysts at 10 mA cm^{-2} typically range from 350 to 430 mV in pH 14 aqueous electrolytes.[15,16] In recent work, Yan showed that hollow spheres of α-$Ni(OH)_2$ catalyzed water oxidation in base with an overpotential of 331 mV at 10 mA cm^{-2} on glassy carbon working electrodes.[17]

Here we report surfactant-free, highly active $[Ni_{1-x}Fe_x(OH)_2](NO_3)_y(OH)_{x-y}{\cdot}nH_2O$ nanosheet water oxidation catalysts with admixed ions. Our best catalyst had an overpotential of 260 mV at 10 mA cm^{-2} on flat highly ordered pyrolytic graphite working electrodes. We attribute the higher activity to unique morphological and structural properties, which were synthetically accessible by the use of pulsed-laser ablation in liquids (PLAL). In PLAL, nanoparticles are formed by very rapid cooling of a plasma comprised of elements from the solid ablation target and the surrounding liquid. This condensation process, which is kinetically controlled, produces predominantly crystalline nanomaterials.[18] PLAL offers size and composition control through a wide range of tunable experimental parameters.[19]

With PLAL, mixed-metal nanomaterials with tailored compositions can be prepared readily by adding metal ions into the aqueous ablation liquid. We intentionally incorporated different amounts of Fe into our α-$Ni(OH)_2$ nanocatalysts, as variable concentrations of Fe in electrodeposited nickel (oxy)hydroxides have been shown to improve electrocatalytic activity.[20−25] We also added Ti^{4+} and La^{3+} ions to the ablation liquid and screened the resulting materials for water oxidation activity.

Eight mixed-metal catalysts were synthesized using PLAL by varying ablation targets, metal ion type and concentrations, and laser pulse energies (see Supporting Information (SI) for experimental details; all ablation solutions contained nitrate). The nanomaterials were prepared with Fe concentrations ranging from 22 to 95% of the total metal content (Table 1). We identified their compositions spectroscopically; notably, they all exhibited high electrocatalytic oxygen-evolution activities in basic electrolytes.

Powder X-ray diffraction (XRD) measurements (SI) indicate that the Fe-rich nanoparticles **1**−**3** are poorly crystalline; the Ni-rich nanoparticles **4**−**8** display diffraction patterns consistent with layered double hydroxide (LDH) structures. XRD data indicate minor contributions from Fe(O)OH;[26] **6** also contained the crystalline spinel $NiFe_2O_4$,[27] and Ti-based oxides

Table 1. Conditions for the Preparation of Catalysts 1−8 and Concentrations of Fe with Respect to Total Metal Content

catalyst	solid target	added ions	ion concn (M)	pulse energy (mJ)	Fe (% metal content)[a]
1	Ni	Fe	0.1	90	95
2	Ni	Fe	0.01	90	86
3	Fe	Ni	0.1	90	70
4	Fe	Ni	1.0	90	36
5	Fe	Ni	3.0	90	22
6	Fe	Ni	3.0	210	30
7	Fe	Ni	3.0	210	23
		Ti	0.015		
8	Fe	Ni	3.0	210	29
		Ti	0.015		
		La	0.023		

[a]Determined by XPS.

Received: June 17, 2014
Published: September 8, 2014

   dx.doi.org/10.1021/ja506087h | J. Am. Chem. Soc. 2014, 136, 13118−13121

were present in **7** and **8**. LDHs have the general formula $[M_{1-x}M'_x(OH)_2](A^{m-})_{x/m}\cdot nH_2O$; the structures are comprised of sheets of $[M_{1-x}M'_x(OH)_2]^{x+}$ edge-shared octahedra. Cationic charges arising from M'^{3+} in the sheets are balanced by intercalated hydrated anions (A^{m-}).[28−30]

X-ray photoelectron spectroscopy (XPS) was employed to obtain binding energies of Ni 2p and Fe 2p core levels in **1**−**8**; these energies are indicative of $Ni(OH)_2$ and (hydrous) iron oxides (SI). In addition, Mössbauer[31,29] and X-ray absorption[32−34] spectroscopic data indicate that Fe is incorporated as Fe^{3+} in place of Ni^{2+} in [Ni-Fe]-LDHs. Two well-resolved N 1s peaks appear in the XP spectra of nanoparticles **4**−**8**, with binding energies of 407.3 and 405.1 eV. The higher binding-energy feature (407.3 eV) is assigned to nitrate.[35−40] The 2.2 eV reduction in N 1s binding energy for the second feature could arise from nitrate in an unusual electronic environment, although nitrogen in a lower oxidation state (e.g., NO_2, NO_2^-) cannot be ruled out. Infrared spectra are consistent with the presence of a second type of NO_x species (SI). Infrared and Raman data (SI) support the presence of intercalated nitrate anions in the LDH structure.[41] On the basis of these data, the predominant crystalline material in **4**−**8** can be assigned to the [Ni-Fe]-LDH $[Ni_{1-x}Fe_x(OH)_2](NO_3)_y(OH)_{x-y}\cdot nH_2O$ (Figure 1).

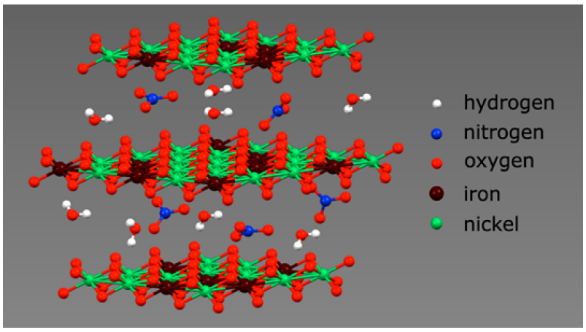

Figure 1. Schematic structural representation of the [Ni-Fe]-LDH $[Ni_{1-x}Fe_x(OH)_2](NO_3)_y(OH)_{x-y}\cdot nH_2O$.

Nanoparticle sizes were obtained from transmission electron micrographs (TEM), and crystalline domain sizes were determined by Scherrer analysis of XRD data. Lateral sizes ranged from ∼7 to 22 nm (Table S1). Catalysts **4** and **5** consisted of nanosheets, as expected for layered structures. Analysis of TEM and XRD data for **6** revealed that two types of nanoparticles were formed; smaller, more spherical (6.5 ± 0.8) nm particles are attributed to the spinel $NiFe_2O_4$, and larger (13 ± 1) nm sheets are assigned to the LDH $[Ni_{1-x}Fe_x(OH)_2](NO_3)_y(OH)_{x-y}\cdot nH_2O$. Also, differences in TEM contrast, shape, and size were found for **7** and **8** (SI).[42] Specific surface areas of catalysts **5** to **8** determined by Brunauer−Emmett−Teller (BET) measurements are in agreement with particle sizes derived from TEM data. Catalysts **6** to **8**, which were synthesized at 210 mJ pulse energy, had similar BET surface areas (193 ± 1 $m^2\ g^{-1}$), whereas **5**, prepared at 90 mJ/pulse, exhibited a slightly higher surface area (220 $m^2\ g^{-1}$) (SI).[43]

We assessed electrocatalytic oxygen-evolution activity in 1 M aqueous KOH.[44] Faradaic yields of oxygen evolution for **5**, **6**, and **8** were all essentially 100%. Steady-state Tafel data were measured to obtain overpotentials; virtually identical mass loadings were used in all electrochemical experiments (all current densities are reported per geometric area). Importantly, chronoamperometry data showed that the catalytic activity of nanoparticles **5**−**8** was maintained for more than 5 h (SI).

The electrocatalytic activities of materials **1**−**5**, synthesized at virtually the same pulse energy, steadily increased with decreasing Fe content (Figure S13). Catalyst **5** (22% Fe relative to total metal content) performed best in the [Ni-Fe]-LDH materials, with an overpotential of 280 mV at 10 mA cm^{-2}. Incorporation of less than 22% Fe relative to total metal content was limited by the solubility of Ni nitrate in the aqueous ablation liquid. XRD data for **5**, collected before and after 30 min of anodic polarization, confirmed that the crystallinity of the [Ni-Fe]-LDH material was retained (Figure S5). The Fe content of our best performing catalyst is in agreement with Dai's report.[34] It differs, however, from findings for amorphous materials, which performed best with 40% Fe.[45]

We made catalyst **6** employing virtually the same precursor conditions as for **5**, but with a pulse energy of 210 instead of 90 mJ. We have shown before with cobalt oxide that pulse energy can be used to control particle size.[19] Varying pulse energy in the synthesis of more complex mixed-metal materials led to particles with different compositions (Figure 2). While **5**

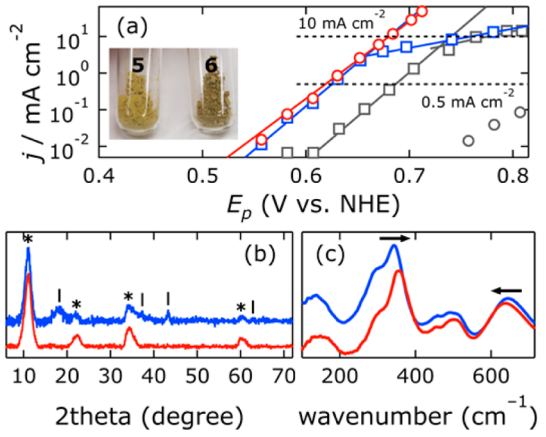

Figure 2. (a) Tafel plots of current density (j) as a function of electrode polarization potential (E_p) (red, **5**; blue, **6**; gray squares, Ni oxide electrodeposited according to ref 50; gray circles, bare electrode), and a photograph of **5** and **6**. (b) XRD data (*, $[Ni_{1-x}Fe_x(OH)_2](NO_3)_y(OH)_{x-y}\cdot nH_2O$; |, $NiFe_2O_4$ spinel). (c) Far-IR spectra (red, **5**; blue, **6**).

consisted mainly of crystalline [Ni-Fe]-LDH, **6** was mixed crystalline [Ni-Fe]-LDH/$NiFe_2O_4$. Catalyst **6** showed inferior activity for water oxidation relative to **5**, presumably because the active [Ni-Fe]-LDH was diluted by the spinel oxide. This finding suggests that crystalline $[Ni_{1-x}Fe_x(OH)_2](NO_3)_y(OH)_{x-y}\cdot nH_2O$ is the more active species in our materials for catalytic water oxidation. IR spectra of **5** and **6** are consistent with $[Ni_{1-x}Fe_x(OH)_2](NO_3)_y(OH)_{x-y}\cdot nH_2O$ with high interstitial water and nitrate content.[46−48] The positions of peaks in the IR spectrum of catalyst **5** indicated the incorporation of Fe into the α-$Ni(OH)_2$ lattice (SI).[49]

The precise nature of the electrocatalytically active species in Fe−Ni−O catalysts has been much discussed.[51,52,45,53] In work on crystalline Fe−Ni−O thin films, Boettcher suggested (Fe,Ni)(O)OH was the catalytically active phase.[24,25] Whereas Dai found that crystalline α-$(Fe,Ni)(OH)_2$ had highest activity with an Fe:Ni ratio of 5:1,[34,54] Hu demonstrated higher intrinsic activity of exfoliated LDHs with a nominal Fe:Ni ratio of 1:3.[55] In other work of note, O'Hare demonstrated that NiTi

dx.doi.org/10.1021/ja506087h | J. Am. Chem. Soc. 2014, 136, 13118−13121

layered double hydroxide nanosheets were effective visible-light-driven water oxidation photocatalysts with $AgNO_3$ as sacrificial electron acceptor.[56]

We found that addition of Lewis-acidic Ti^{4+} and La^{3+} ions to the ablation liquid improved catalytic activity relative to our most active [Fe-Ni]-LDH catalyst (**5**). We synthesized catalysts **7** and **8** using virtually the same precursor conditions as for **5**, but with Ti^{4+} (**7**) or Ti^{4+} and La^{3+} (**8**) added to the ablation solution (Table 1). XRD data revealed that both catalysts were primarily [Ni-Fe]-LDH materials (SI). Oxides containing added elements were also present; TiO_2 and Fe_2TiO_4 were found in **7**, whereas crystalline Ni_3TiO_5 and $La(Ni,Fe)O_3$ were detected in **8**. The spinel oxide $NiFe_2O_4$ was absent from both **7** and **8**. XPS data showed that **8** contained 1% La relative to total metal content. Both catalysts were more active than LDHs **5** and **6**, with **7** and **8** exhibiting the lowest overpotentials at 10 mA cm^{-2} of 270 and 260 mV, respectively (SI).

Highly active, surfactant-free, mixed transition metal hydroxide water oxidation nanoparticle catalysts can be made by PLAL. We spectroscopically identified a crystalline [Ni-Fe]-LDH as the catalytically most active material. We discovered that turnover frequency correlated with the ratio of two nitrogen species detected by XPS in the as-synthesized catalysts (Figure 3). Addition of Ti^{4+} and La^{3+} ions further enhanced

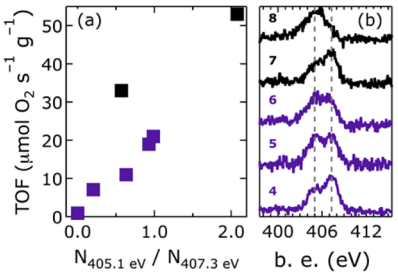

Figure 3. (a) Turnover frequency vs $N_{405.1eV}/N_{407.3eV}$ (purple, neat Fe−Ni-based catalysts; black, **7** and **8**). (b) XPS data of catalysts **4**−**8**; the gray dashed lines mark the N 1s binding energies (405.1 and 407.3 eV).

activity (reaching 10 mA cm^{-2} at an overpotential of 260 mV). On a flat electrode, this is the lowest overpotential reported to date for mixed metal oxide catalysts.

■ ASSOCIATED CONTENT

Ⓢ Supporting Information

General experimental conditions and apparatus; physical and electrochemical characterization. This material is available free of charge via the Internet at http://pubs.acs.org.

■ AUTHOR INFORMATION

Corresponding Author

astridm@caltech.edu

Notes

The authors' institution (California Institute of Technology) has filed a provisional U.S. patent application directly relating to the work described in the manuscript (provisional patent application no. 62/013,976; filed on June 18, 2014).

■ ACKNOWLEDGMENTS

We thank Richard Gerhart for fabrication of an electrochemical cell, Alasdair McDowall for help with TEM, and George Rossman for help with solid-state Raman and IR spectroscopies. Research was carried out in the Laser Resource Center and the Molecular Materials Research Center of the Beckman Institute of the California Institute of Technology. This work was supported by the NSF CCI Solar Fuels Program (CHE-1305124) and the Arnold and Mabel Beckman Foundation.

■ REFERENCES

(1) Gray, H. B. *Nature Chem.* **2009**, *1*, 7.
(2) Lewis, N. S.; Nocera, D. G. *Proc. Natl. Acad. Sci. U.S.A.* **2006**, *103*, 15729.
(3) Walter, M. G.; Warren, E. L.; McKone, J. R.; Boettcher, S. W.; Mi, Q.; Santori, E. A.; Lewis, N. S. *Chem. Rev.* **2010**, *110*, 6446.
(4) McKone, J. R.; Lewis, N. S.; Gray, H. B. *Chem. Mater.* **2013**, *26*, 407.
(5) Trasatti, S. *Electrochim. Acta* **1984**, *29*, 1503.
(6) Man, I. C.; Su, H.-Y.; Calle-Vallejo, F.; Hansen, H. A.; Martínez, J. I.; Inoglu, N. G.; Kitchin, J.; Jaramillo, T. F.; Nørskov, J. K.; Rossmeisl, J. *ChemCatChem* **2011**, *3*, 1159.
(7) Gilbert, J. A.; Eggleston, D. S.; Murphy, W. R.; Geselowitz, D. A.; Gersten, S. W.; Hodgson, D. J.; Meyer, T. J. *J. Am. Chem. Soc.* **1985**, *107*, 3855.
(8) Limburg, J.; Brudvig, G. W.; Crabtree, R. H. *J. Am. Chem. Soc.* **1997**, *119*, 2761.
(9) Ruettinger, W.; Yagi, M.; Wolf, K.; Bernasek, S.; Dismukes, G. C. *J. Am. Chem. Soc.* **2000**, *122*, 10353.
(10) Dau, H.; Limberg, C.; Reier, T.; Risch, M.; Roggan, S.; Strasser, P. *ChemCatChem* **2010**, *2*, 724.
(11) Yin, Q.; Tan, J. M.; Besson, C.; Geletii, Y. V.; Musaev, D. G.; Kuznetsov, A. E.; Luo, Z.; Hardcastle, K. I.; Hill, C. L. *Science* **2010**, *328*, 342.
(12) Wiechen, M.; Zaharieva, I.; Dau, H.; Kurz, P. *Chem. Sci.* **2012**, *3*, 2330.
(13) Du, P.; Eisenberg, R. *Energy Environ. Sci.* **2012**, *5*, 6012.
(14) Singh, A.; Spiccia, L. *Coord. Chem. Rev.* **2013**, *257*, 2607.
(15) McCrory, C. C. L.; Jung, S.; Peters, J. C.; Jaramillo, T. F. *J. Am. Chem. Soc.* **2013**, *135*, 16977.
(16) Yang recently reported a highly active graphene FeNi double hydroxide hybrid on Ni foam working electrodes: Long, X.; Li, J.; Xiao, S.; Yan, K.; Wang, Z.; Chen, H.; Yang, S. *Angew. Chem., Int. Ed.* **2014**, *53*, 7584. However, the high porosity of the electrode substrate leads to a surface area enlargement, inflating current densities that were normalized to the geometric electrode area; this makes a performance comparison impossible.
(17) Gao, M.; Sheng, W.; Zhuang, Z.; Fang, Q.; Gu, S.; Jiang, J.; Yan, Y. *J. Am. Chem. Soc.* **2014**, *136*, 7077.
(18) Yang, G. W. *Prog. Mater. Sci.* **2007**, *52*, 648.
(19) Blakemore, J. D.; Gray, H. B.; Winkler, J. R.; Müller, A. M. *ACS Catal.* **2013**, *3*, 2497.
(20) Corrigan, D. A. *J. Electrochem. Soc.* **1987**, *134*, 377.
(21) Risch, M.; Klingan, K.; Heidkamp, J.; Ehrenberg, D.; Chernev, P.; Zaharieva, I.; Dau, H. *Chem. Commun.* **2011**, *47*, 11912.
(22) Li, X.; Walsh, F. C.; Pletcher, D. *Phys. Chem. Chem. Phys.* **2011**, *13*, 1162.
(23) Lyons, M. E. G.; Cakara, A.; O'Brien, P.; Godwin, I.; Doyle, R. L. *Int. J. Electrochem. Sci.* **2012**, *7*, 11768.
(24) Trotochaud, L.; Ranney, J. K.; Williams, K. N.; Boettcher, S. W. *J. Am. Chem. Soc.* **2012**, *134*, 17253.
(25) Trotochaud, L.; Young, S. L.; Ranney, J. K.; Boettcher, S. W. *J. Am. Chem. Soc.* **2014**, *136*, 6744.
(26) Powder diffraction file no. 00-029-0713 (ICDD, 2012).
(27) Powder diffraction file no. 01-076-6119 (ICDD, 2012).
(28) Demourgues-Guerlou, L.; Fournès, L.; Delmas, C. *J. Solid State Chem.* **1995**, *114*, 6.
(29) Axmann, P.; Glemser, O. *J. Alloys Compd.* **1997**, *246*, 232.
(30) Trolard, F.; Bourrié, G. In *Clay Minerals in Nature—Their Characterization, Modification and Application*; Valaskova, M., Ed.; InTech: Ostrava, Czech Republic, 2012.

(31) Corrigan, D. A.; Conell, R. S.; Fierro, C. A.; Scherson, D. A. *J. Phys. Chem.* **1987**, *91*, 5009.
(32) Balasubramanian, M.; Melendres, C. A.; Mini, S. *J. Phys. Chem. B* **2000**, *104*, 4300.
(33) Landon, J.; Demeter, E.; İnoğlu, N.; Keturakis, C.; Wachs, I. E.; Vasić, R.; Frenkel, A. I.; Kitchin, J. R. *ACS Catal.* **2012**, *2*, 1793.
(34) Gong, M.; Li, Y.; Wang, H.; Liang, Y.; Wu, J. Z.; Zhou, J.; Wang, J.; Regier, T.; Wei, F.; Dai, H. *J. Am. Chem. Soc.* **2013**, *135*, 8452.
(35) Wagner, C. D.; Riggs, W. M.; Davis, L. E.; Moulder,J. F. In *Handbook of X-Ray Photoelectron Spectroscopy*, 1st ed.; Mullenberg, G. E., Ed.; Perkin-Elmer Corp.: Eden Prairie, MN, 1979.
(36) Bandis, C.; Scudiero, L.; Langford, S. C.; Dickinson, J. T. *Surf. Sci.* **1999**, *442*, 413.
(37) Wei, M.; Xu, X.; Wang, X.; Li, F.; Zhang, H.; Lu, Y.; Pu, M.; Evans, D. G.; Duan, X. *Eur. J. Inorg. Chem.* **2006**, *2006*, 2831.
(38) Baltrusaitis, J.; Jayaweera, P. M.; Grassian, V. H. *Phys. Chem. Chem. Phys.* **2009**, *11*, 8295.
(39) Wang, X.; Deng, R.; Kulkarni, S. A.; Wang, X.; Pramana, S. S.; Wong, C. C.; Gratzel, M.; Uchida, S.; Mhaisalkar, S. G. *J. Mater. Chem. A* **2013**, *1*, 4345.
(40) Nanayakkara, C. E.; Jayaweera, P. M.; Rubasinghege, G.; Baltrusaitis, J.; Grassian, V. H. *J. Phys. Chem. A* **2013**, *118*, 158.
(41) Frost, R. L.; Erickson, K. L.; Kloprogge, T. J. *Spectrochim. Acta, Part A* **2005**, *61*, 2919.
(42) Co-crystallization of several crystal phases cannot be excluded in such small size domains.
(43) We note that, strictly speaking, BET surface areas are not necessarily equivalent to electroactive surface areas.
(44) Pourbaix, M. *Atlas of Electrochemical Equilibria in Aqueous Solutions*; Pergamon Press: New York, 1966.
(45) Louie, M. W.; Bell, A. T. *J. Am. Chem. Soc.* **2013**, *135*, 12329.
(46) Oliva, P.; Leonardi, J.; Laurent, J. F.; Delmas, C.; Braconnier, J. J.; Figlarz, M.; Fievet, F.; Guibert, A. d. *J. Power Sources* **1982**, *8*, 229.
(47) Kermarec, M.; Carriat, J. Y.; Burattin, P.; Che, M.; Decarreau, A. *J. Phys. Chem.* **1994**, *98*, 12008.
(48) Hall, D. S.; Lockwood, D. J.; Poirier, S.; Bock, C.; MacDougall, B. R. *J. Phys. Chem. A* **2012**, *116*, 6771.
(49) Hannoyer, B.; Ristić, M.; Popović, S.; Musić, S.; Petit, F.; Foulon, B.; Dalipi, S. *Mater. Chem. Phys.* **1998**, *55*, 215.
(50) Dincă, M.; Surendranath, Y.; Nocera, D. G. *Proc. Natl. Acad. Sci. U.S.A.* **2010**, *107*, 10337.
(51) Bediako, D. K.; Lassalle-Kaiser, B.; Surendranath, Y.; Yano, J.; Yachandra, V. K.; Nocera, D. G. *J. Am. Chem. Soc.* **2012**, *134*, 6801.
(52) Smith, R. D. L.; Prévot, M. S.; Fagan, R. D.; Trudel, S.; Berlinguette, C. P. *J. Am. Chem. Soc.* **2013**, *135*, 11580.
(53) Chen, J. Y. C.; Miller, J. T.; Gerken, J. B.; Stahl, S. S. *Energy Environ. Sci.* **2014**, *7*, 1382.
(54) For a comparison of activities see Table S3.
(55) Song, F.; Hu, X. *Nat. Commun.* **2014**, *5*, No. 4477.
(56) Zhao, Y.; Li, B.; Wang, Q.; Gao, W.; Wang, C. J.; Wei, M.; Evans, D. G.; Duan, X.; O'Hare, D. *Chem. Sci.* **2014**, *5*, 951.